Benzylidene-Directed Glycosylations – Mechanistic Insights from Cryogenic Infrared Spectroscopy

Kevin Pagel (kevin.pagel@fu-berlin.de)
Freie Universität Berlin https://orcid.org/0000-0001-8054-4718
Chun-Wei Chang
Freie Universität Berlin https://orcid.org/0000-0002-0253-3463
Kim Greis
Freie Universität Berlin
Carla Kirschbaum
Freie Universität Berlin
Sabrina Leichnitz
Max Planck Institute of Colloids and Interfaces
Gerard Meijer
Fritz-Haber-Institut der Max-Planck-Gesellschaft
Gert von Helden
Fritz-Haber-Institut der Max-Planck-Gesellschaft
Peter Seeberger
Max Planck Institute of Colloids and Interfaces

Article

Keywords:

Posted Date: November 2nd, 2023

DOI: https://doi.org/10.21203/rs.3.rs-3512691/v1

Additional Declarations: There is **NO** Competing Interest.

Abstract

The stereoselective formation of 1,2-*cis* glycosidic linkages is challenging. The currently most widely used strategy for their installation uses 4,6-*O*-benzylidene protected building blocks. The stereoselectivity of this reaction is thought to be driven by a covalent intermediate, which reacts *via* an S_N2 mechanism. However, the role of cationic S_N1-type intermediates in this reaction is unclear. Here, we elucidate the structure of glycosyl cations carrying 4,6-*O*-benzylidene groups using cryogenic infrared ion spectroscopy and computational methods. The data reveal that the intermediates unexpectedly form anhydro cations, which correlates well with the stereoselective outcome of S_N1-type glycosylations. The study highlights how cryogenic infrared spectroscopy can unravel novel intermediates in sugar chemistry and how this structural data can be linked to reactions in solution.

Full Text

Carbohydrates are ubiquitous in nature and are essential for many biological events. Specific 1,2-*cis* or -*trans* linkages are crucial for a variety of recognition processes and play a central role during viral infections.[1,2] Accessing pure oligosaccharides through chemical synthesis is challenging. The regiochemistry has to be controlled via an elaborate protecting group strategy; the emergence of a new chiral center during glycosidic bond formation complicates stereocontrol at the anomeric carbon. 1,2-*trans* glycosides can be readily obtained using neighboring group participation.[3] In contrast, 1,2-*cis* selectivity is much more difficult to achieve because there is no universal method to reliably construct 1,2-*cis* glycosidic bonds.[4,5]

A better understanding of the reaction mechanism can help to optimize reaction conditions.[3,6-10] The mechanism of glycosylation reactions is a continuum between two extremes: an S_N1-type mechanism involving a cationic intermediate on one hand, and an S_N2-type reaction with a penta-coordinated transition state on the other (Figure 1a).[10,11] α-Glycosyl triflates in combination with strong nucleophiles almost exclusively lead to β-glycosides *via* an S_N2 mechanism, as first discovered by Crich.[11-13] Experiments using isotopically labeled glycosylating agents further provided evidence for the generation of α-selective β-triflates.[14] However, it was also suggested that weak nucleophiles may not react *via* an S_N2 mechanism.[15] Instead, the reaction mechanism shifts to a dissociative S_N1 pathway, in which transient cationic intermediates favor an α-nucleophilic addition due to the anomeric effect.[16]

A promising method to preferentially obtain 1,2-*cis* glycosides are 4,6-*O*-benzylidene directed glycosylations, which were initially introduced by Crich[17,18] and further refined by Wang and Codée (Figure 1b).[19-22] With strong nucleophiles, such as methanol, the obtained α-selectivity is low (<20%). However, the α-selectivity gradually increases with weaker nucleophiles, such as isopropanol or monosaccharides. Strong nucleophiles therefore favor an S_N2-type reaction, whereas weak nucleophiles more likely react *via* an S_N1 mechanism. The increase in α-selectivity is significantly different for

galactose (Gal), glucose (Glc), and mannose (Man). Galactose shows the highest α-selectivity with up to 100%, while glucose and mannose only reach between 40% and 50%. This distinct selectivity is arising from a delicate interplay between different factors such as the anomeric effect, the structure of the oxocarbenium ion and the presence of other highly reactive species.

A detailed structural understanding of the reaction intermediates is essential to understand the glycosylation mechanism. Previously, the S_N2 mechanism and its α-glycosyl triflate intermediate were studied using nuclear magnetic resonance (NMR) spectroscopy.[14,18,23,24] In contrast, the intermediate of S_N1-type glycosylation reactions – the glycosyl cation – is inaccessible to traditional spectroscopic techniques because of its short lifetime (picoseconds).[23,25] Nevertheless, valuable information on the S_N1 trajectory has been obtained using density functional theory (DFT),[26,27] kinetic isotope experiments,[18,28] cation clock reactions,[29,30] and NMR in super-acid media.[31] Despite these significant advances, no direct structural data of glycosyl cations in benzylidene-mediated glycosylations have been obtained so far.

Gas-phase spectroscopy is a powerful tool for the structural characterization of glycosyl cations.[3,6-8,32-38] Here, we use a combination of cryogenic infrared (IR) spectroscopy in helium droplets and DFT to unravel the structure of glycosyl cations generated from 4,6-*O*-benzylidene protected building blocks. Our data suggest that the intermediate forms an anhydro cation, which correlates with the stereoselective outcome observed for 4,6-*O*-benzylidene protected glycosylating agents in combination with weak nucleophiles.

The experimental setup has been described in detail previously (see Supporting Information).[39-41] Briefly, glycosyl precursors are ionized and transferred into the gas phase by nano-electrospray ionization (nESI). In-source fragmentation cleaves the leaving group at C1 to generate glycosyl cations. Subsequently, mass-to-charge selected glycosyl cations are guided into a hexapole ion trap. A coaxial beam of superfluid helium nanodroplets (0.37 K) picks up the ions and transports them from the trap to a detection region. Here, the droplets overlap with an IR beam generated by the Fritz Haber Institute Free-Electron Laser (FHI-FEL).[42] Sequential absorption of multiple resonant photons leads to evaporation of the helium shell and ejection of the ions, which are detected by a time-of-flight mass analyzer. The ion count as a function of the laser wavelength leads to a highly resolved IR spectrum. The experimental vibrational spectra can be linked to a glycosyl cation structure using DFT calculations. A conformational search using CREST[43] with the semi-empirical method GFN2-xTB[44] yielded over 300 structures for each intermediate. Free energies and harmonic frequencies were computed at the PBE0+D3/6-311+G(d,p)[45,46] level of theory in Gaussian 16.[47]

Electrospray ionization and in-source fragmentation of the thioethyl glucoside **Glc-SEt** leads to cleavage of the thioethyl (SEt) group and the formation of a glycosyl cation (Figure 2a). Subsequently, the intermediate is trapped, and its IR spectrum recorded in the 1000–1800 cm^{-1} range (Figure 2b). Initially, it was expected that the vibrational signature correspond to an oxocarbenium-type ion **Glc-oxo** (Figure 2b,

green), which is a commonly suggested intermediate.[10,11,23] Surprisingly, oxocarbenium ions are not formed, because the characteristic C_1=O_5 stretching vibration in the experimental spectrum around 1500 cm^{-1} is clearly missing.[3,6] Instead, the experimental spectrum is most consistent with the lowest-energy computed spectrum of an 1,6-anhydro cation **Glc-6B**. Here, the benzylidene protecting group splits into a hydroxylate moiety at C6, which forms a covalent bond to the anomeric carbon, and a benzylium moiety ($PhCHO^+$) at C4 (Figure 2b, blue). Anhydro cations are significantly more stable than oxocarbenium ions, due to delocalization of the positive charge in the $PhCHO^+$ moiety. The characteristic IR pattern of anhydro cations falls into two main regions: the absorption of the benzylic carbocation in the higher frequency region (1400–1650 cm^{-1}) and the C–O and C–C stretching as well as C–H bending modes below 1400 cm^{-1}. Five major bands originating from the $PhCHO^+$ moiety are diagnostic for anhydro cations: 1) the feature at 1557 cm^{-1}, which corresponds to the C=O^+ stretch of the benzylium moiety the bands at 2) 1610 and 3) 1579 cm^{-1} which are symmetric and antisymmetric C=C stretches within the phenyl ring, and the diagnostic vibrations at 4) 1437 and 5) 1408 cm^{-1} which are C–H bends of the CHO^+ and the Ph moieties, respectively. Energetically, **Glc-6B** is found to be 73 kJ mol^{-1} more stable than the oxocarbenium ion **Glc-oxo**. The formation of an alternative 1,4-anhydro cation **Glc-4B**, where the generated hydroxylate group is at C4 (Figure 2b, red), is conceivable as well. Its harmonic frequencies partially match the experimental IR spectrum, however, it overall matches less well than **Glc-6B** and is 28 kJ mol^{-1} less stable.

The rearrangement of a 4,6-*O*-benzylidene system into anhydro cations is particularly surprising because the 4,6-*O*-benzylidene acetal moiety is considered non-participating. That is, it is expected to interact with the anomeric carbon. The formation of anhydro cations not only results in a significant energetic stabilization of the intermediate but also twists the sugar into a more rigid [3.2.1]-bicyclic backbone.[48] As a result, all functional groups are reoriented into the rather unusual axial/pseudo-axial positions.

A clear correlation between the structure of the gas-phase intermediate and the stereoselectivity of the condensed-phase products is observed. In the solution-phase glycosylation reactions, the α-content gradually increases when weak nucleophiles are used.[21,22] Under these conditions an S_N1 mechanism and the formation of a positively charged intermediate is likely. In the 1,6-anhydro cations experimentally detected here, the β-face is shielded, and a nucleophilic attack is favored from the α-side. The 1,4-anhydro cations on the other hand have potential β-selectivity. However the high relative energy level suggests that these intermediates are not particularly abundant. Taken together, the formation of anhydro cations in condensed-phase S_N1-type glycosylations could explain the increased content of α-products. However, an involvement of β-triflates in these α-glycosylations cannot be ruled out based on this data.[14]

Similarly to the glucose intermediate, no indication for the presence of oxocarbenium-type structures **Man-oxo** is observed for the corresponding 4,6-*O*-benzylidene mannosyl cation (Figure S2a). Instead, the comparison between experiment and theory suggests the formation of an anhydro cation as well (Figure 3a). The lowest-energy oxocarbenium-type structure is 73 kJ mol^{-1} less stable than the

lowest-energy **Man-4B** 1,4-anhydro cation ($B_{1,4}$, 0 kJ mol^{-1}). The harmonic frequencies of this cation as well as those of its 1,6-anhydro counterpart **Man-6B** ($B_{o,3}$, +12 kJ mol^{-1}) match the experiment comparably well. Although **Man-4B** is lower in energy, it is possible that both ions are generated in the experiment. As for glucose, the vibrational modes associated with the $PhCHO^+$ moiety in the 1400–1650 cm^{-1} region are the major diagnostic features for the formation of anhydro cations. The main difference to the glucosyl cation spectrum is found in the fingerprint region (1000–1200 cm^{-1}).

In the condensed phase, the mannosyl building block is more β-selective than its glucose counterpart when weak nucleophiles are used (Figure 1B). Interestingly, the formation of the anhydro ring in the lowest-energy structure **Man-4B** leads to shielding of the α-side and a preferential nucleophilic attack from the β-side. The selectivity of this structure aligns well to the β-selectivity observed in benzylidene-directed mannosylatios.[17-19,21] The less stable **Man-6B**, on the other hand, would rather induce the formation of α-mannosides. One could speculate that the higher α-selectivity observed in glucose compared to mannose can be attributed to the involvement of both intermediates. Specifically, the higher stability of **Glc-6B** compared to **Glc-4B** promotes a greater α-content. Conversely, the prevalence of β-mannosylation could be influenced by the higher thermodynamic stability of **Man-4B** in comparison to **Man-6B**.

For galactose, the computed spectra (Figure 3b) of two anhydro cations **Gal-6B** ($^4C_1$, 0 kJ mol^{-1}) and **Gal-4B** (^{1,4}B, +8 kJ mol^{-1}) are close to the experimental IR spectrum, comparing to **Gla-oxo**. As for the other sugars, anhydro galactose cations are energetically preferred over oxocarbenium ions (+29 kJ mol^{-1}). Although the two anhydro cations are structurally different, their computed free energies are similar with **Gal-4B** being 8 kJ mol^{-1} less stable than **Gal-6B**. In contrast to to Glc and Man, however, the b-side of the anomeric carbon is blocked in both structures **Gal-6B** and **Gal-4B.** This implies a pronounced α-selectivity in galactosylations with weak nucleophiles. Surprisingly, this is exactly what is observed in condensed-phase reactions using 4,6-*O*-benzylidene galactosyl building blocks, which show almost 100% α-selectivity (Figure 1b).[49]

The correlation between gas-phase and condensed-phase structures is the subject of intense debate[50,51] and was studied by many synthetic[8,23,34-36,52-54] and physical chemistry laboratories[3,6,7,33,37,38,41] Here, the structure of glycosyl cations is probed in the vacuum of a mass spectrometer (relative permittivity ε_r = 1), which is considerably different to an aqueous solution (ε_r = 80). However, typical glycosylation reactions are not performed in water. Instead, highly apolar solvents, such as toluene (ε_r = 2.4) or dichloromethane (ε_r = 8.9), with a relative permittivity close to that of vacuum are used. The presented structural data are therefore potentially relevant for typical reactions in glycochemistry.

To test the impact of the solvent on the relative stability of the generated intermediates, the calculated structures were reoptimized using the COSMO solvation model[55,56] for various solvents with distinct relative permittivities (Figure 3c and Supporting Information). The free energies of the most stable

glycosyl cations with a solvent model are compared to those of the gas-phase structures. The results suggest that anhydro cations are not only the most stable structures in the gas phase but also retain their stability when a solvent model is introduced. Further, the computational data shows that upon solvation the ring puckers largely remain identical to those adopted in the gas phase, whereas the side chains (OBn) orient differently. These results are in line with previous studies,[57,58] where IR spectra of other intermediates were found to be nearly identical, regardless whether they were probed in solution or in the gas phase.

In conclusion, we present here the first direct structural characterization of glycosyl cation intermediates generated from benzylidene-protected glycosylating agents. The presented structures were derived by matching cryogenic gas-phase IR spectra with computed harmonic frequencies obtained from DFT calculations. For glucose, galactose, and mannose, the intermediates unexpectedly form anhydro cations. The anhydro cation formation likely involves two steps (Figure 3d): (1) the oxocarbenium ion undergoes a ring-opening reaction of the benzylidene acetal at O4 or O6 to generate a zwitterionic species.[59] (2) O6 or O4 remote participation leads to the formation of an anhydro ring.[6] The obtained structures show a clear connection between the structure of the intermediates and the stereoselective outcome in glycosylation reactions. The inverse selectivities of the anhydro cations correlates well with the mixed anomer ratios that are observed when benzylidene-protected building blocks are used under conditions that favor an S_N1-type glycosylation. Computations on glycosyl cations with a solvent model furthermore reveal a high degree of similarity between the gas- and condensed-phase structures. The structural insights reported here provide a plausible mechanistic explanation of the S_N1-type reactivity in benzylidene-directed glycosylations and can serve as a guideline to fine tune their reactivity on the road to 1,2-*cis* selective glycosylation reactions.

Declarations

Acknowledgements

The authors gratefully acknowledge generous funding by the Max-Planck-Society and Freie Universität Berlin. K.P. acknowledges generous funding by the European Research Council, ERC-2019-CoG-863934-GlycoSpec.

Author contributions

K.P. designed and directed the research and supervised the project. C.W.C performed quantum chemical calculations and conducted chemical synthesis. K. G. and C. K. acquired cryogenic infrared spectroscopy. All authors wrote the manuscript, analyzed data, and interpreted the results.

Competing interests

The authors declare no competing interests.

References

1. Boltje, T. J., Buskas, T. & Boons, G.-J. Opportunities and Challenges in Synthetic Oligosaccharide and Glycoconjugate Research. *Nat. Chem.* **1**, 611-622 (2009).
2. Seeberger, P. H. Chemical Glycobiology: Why Now? *Nat. Chem. Biol.* **5**, 368-372 (2009).
3. Mucha, E. *et al.* Unravelling the Structure of Glycosyl Cations via Cold-ion Infrared Spectroscopy. *Nat. Commun.* **9**, 4174 (2018).
4. Panza, M., Pistorio, S. G., Stine, K. J. & Demchenko, A. V. Automated Chemical Oligosaccharide Synthesis: Novel Approach to Traditional Challenges. *Chem. Rev.* **118**, 8105-8150 (2018).
5. Kulkarni, S. S. *et al.* "One-pot" Protection, Glycosylation, and Protection–glycosylation Strategies of Carbohydrates. *Chem. Rev.* **118**, 8025-8104 (2018).
6. Marianski, M. *et al.* Remote Participation during Glycosylation Reactions of Galactose Building Blocks: Direct Evidence from Cryogenic Vibrational Spectroscopy. *Angew. Chem. Int. Ed.* **59**, 6166-6171 (2020).
7. Greis, K. *et al.* The Influence of the Electron Density in Acyl Protecting Groups on the Selectivity of Galactose Formation. *J. Am. Chem. Soc.* **144**, 20258-20266 (2022).
8. Braak, F. t. *et al.* Characterization of Elusive Reaction Intermediates Using Infrared Ion Spectroscopy: Application to the Experimental Characterization of Glycosyl Cations. *Acc. Chem. Res.* **55**, 1669-1679 (2022).
9. Adero, P. O., Amarasekara, H., Wen, P., Bohé, L. & Crich, D. The Experimental Evidence in Support of Glycosylation Mechanisms at the S_N1–S_N2 interface. *Chem. Rev.* **118**, 8242-8284 (2018).
10. Hettikankanamalage, A. A., Lassfolk, R., Ekholm, F. S., Leino, R. & Crich, D. Mechanisms of Stereodirecting Participation and Ester Migration from Near and Far in Glycosylation and Related Reactions. *Chem. Rev.* **120**, 7104-7151 (2020).
11. Crich, D. Mechanism of a Chemical Glycosylation Reaction. *Acc. Chem. Res.* **43**, 1144-1153 (2010).
12. Crich, D. & Sun, S. Are Glycosyl Triflates Intermediates in the Sulfoxide Glycosylation Method? A Chemical and ^{1}H, ^{13}C, and ^{19}F NMR Spectroscopic Investigation. *J. Am. Chem. Soc.* **119**, 11217-11223 (1997).
13. Frihed, T. G., Bols, M. & Pedersen, C. M. Mechanisms of Glycosylation Reactions Studied by Low-temperature Nuclear Magnetic Resonance. *Chem. Rev.* **115**, 4963-5013 (2015).
14. Santana, A. G. *et al.* Dissecting the Essential Role of Anomeric b-Triflates in Glycosylation Reactions. *J. Am. Chem. Soc.* **142**, 12501-12514 (2020).
15. van der Vorm, S. *et al.* Acceptor Reactivity in Glycosylation Reactions. *Chem. Soc. Rev.* **48**, 4688-4706 (2019).
16. Alabugin, I. V., Manoharan, M. & Zeidan, T. A. Homoanomeric Effects in Six-Membered Heterocycles. *J. Am. Chem. Soc.* **125**, 14014-14031 (2003).

17. Crich, D. En Route to the Transformation of Glycoscience: A Chemist's Perspective on Internal and External Crossroads in Glycochemistry. *J. Am. Chem. Soc.* **143**, 17-34 (2020).
18. Huang, M. *et al.* Dissecting the Mechanisms of a Class of Chemical Glycosylation using Primary ^{13}C Kinetic Isotope Effects. *Nat. Chem.* **4**, 663-667 (2012).
19. van der Vorm, S., Hansen, T., Overkleeft, H. S., van der Marel, G. A. & Codée, J. D. C. The Influence of Acceptor Nucleophilicity on the Glycosylation Reaction Mechanism. *Chem. Sci.* **8**, 1867-1875 (2017).
20. van der Vorm, S. *et al.* Mapping the Relationship between Glycosyl Acceptor Reactivity and Glycosylation Stereoselectivity. *Angew. Chem. Int. Ed.* **57**, 8240-8244 (2018).
21. Chang, C.-W. *et al.* Establishment of Guidelines for the Control of Glycosylation Reactions and Intermediates by Quantitative Assessment of Reactivity. *Angew. Chem. Int. Ed.* **58**, 16775-16779 (2019).
22. Chang, C.-W. *et al.* Automated Quantification of Hydroxyl Reactivities: Prediction of Glycosylation Reactions. *Angew. Chem. Int. Ed.* **60**, 12413-12423 (2021).
23. Franconetti, A. *et al.* Glycosyl Oxocarbenium Ions: Structure, Conformation, Reactivity, and Interactions. *Acc. Chem. Res.* **54**, 2552-2564 (2021).
24. Chang, C.-W. *et al.* Unraveling the Promoter Effect and the Roles of Counterion Exchange in Glycosylation Reaction. *Sci. Adv.* **9**, eadk0531 (2023).
25. Amyes, T. L. & Jencks, W. P. Lifetimes of oxocarbenium ions in aqueous solution from common ion inhibition of the solvolysis of .alpha.-azido ethers by added azide ion. *J. Am. Chem. Soc.* **111**, 7888-7900 (1989).
26. Merino, P. *et al.* Computational Evidence of Glycosyl Cations. *Org. Biomol. Chem.* **19**, 2350-2365 (2021).
27. Hansen, T. *et al.* Defining the S_N1 Side of Glycosylation Reactions: Stereoselectivity of Glycopyranosyl Cations. *ACS Cent. Sci.* **5**, 781-788 (2019).
28. Zhuo, M. H., Wilbur, D. J., Kwan, E. E. & Bennett, C. S. Matching glycosyl donor reactivity to sulfonate leaving group ability permits S_N2 glycosylations. *J. Am. Chem. Soc.* **141**, 16743-16754 (2019).
29. Adero, P. O. *et al.* Cation Clock Reactions for the Determination of Relative Reaction Kinetics in Glycosylation Reactions: Applications to Gluco- and Mannopyranosyl Sulfoxide and Trichloroacetimidate Type Donors. *J. Am. Chem. Soc.* **137**, 10336-10345 (2015).
30. Huang, M., Retailleau, P., Bohé, L. & Crich, D. Cation Clock Permits Sistinction Between the Mechanisms of α- and β-*O*- and β-*C*-Glycosylation in the Mannopyranose Series: Evidence for the Existence of a Mannopyranosyl Oxocarbenium Ion. *J. Am. Chem. Soc.* **134**, 14746-14749 (2012).
31. Martin, A. *et al.* Catching elusive glycosyl cations in a condensed phase with HF/SbF_5 superacid. *Nat. Chem.* **8**, 186-191 (2016).
32. Greis, K. *et al.* Studying the Key Intermediate of RNA Autohydrolysis by Cryogenic Gas-Phase Infrared Spectroscopy. *Angew. Chem. Int. Ed.* **61**, e2021154 (2022).

33. Greis, K. *et al.* Neighboring Group Participation of Benzoyl Protecting Groups in C3- and C6-Fluorinated Glucose. *Eur. J. Org. Chem.* **2022**, e202200255 (2022).
34. Hansen, T. *et al.* Characterization of Glycosyl Dioxolenium Ions and Their Role in Glycosylation Reactions. *Nat. Commun.* **11**, 2664 (2020).
35. Remmerswaal, W. A. *et al.* Stabilization of Glucosyl Dioxolenium Ions by “Dual Participation” of the 2,2-Dimethyl-2-(ortho-nitrophenyl)acetyl (DMNPA) Protection Group for 1,2-cis-Glucosylation. *J. Org. Chem.* **87**, 9139-9147 (2022).
36. Elferink, H. *et al.* Direct Experimental Characterization of Glycosyl Cations by Infrared Ion Spectroscopy. *J. Am. Chem. Soc.* **140**, 6034-6038 (2018).
37. Greis, K. *et al.* Direct Experimental Characterization of the Ferrier Glycosyl Cation in the Gas Phase. *Org. Lett.* **22**, 8916-8919 (2020).
38. Greis, K. *et al.* The Impact of Leaving Group Anomericity on the Structure of Glycosyl Cations of Protected Galactosides. *ChemPhysChem* **21**, 1905-1907 (2020).
39. Greis, K., Kirschbaum, C., von Helden, G. & Pagel, K. Gas-phase Infrared Spectroscopy of Glycans and Glycoconjugates. *Curr. Opin. Struct. Biol.* **72**, 194-202 (2022).
40. Gray, C. J. *et al.* Advancing Solutions to the Carbohydrate Sequencing Challenge. *J. Am. Chem. Soc.* **141**, 14463-14479 (2019).

Methods

The precursors were dissolved in a 9:1 (V:V) mixture of acetonitrile and water to yield 0.1 mM solutions. Pd/Pt coated glass capillaries (Sputter Coater HR 208, *Cressington*) for nano electrospray ionization (nESI) are pulled to a tip with an inner diameter of 1–2 µm using a micropipette puller (Model P-1000, *Sutter Instrument*). Glycosyl cations were generated and probed using a custom-built helium droplet instrument. Glycosyl cations are formed after nESI (Z-spray) with a voltage of 1.1 kV to the tip of the capillary of the precursors, followed by in-source fragmentation of the generated ions. Commonly, nESI of the precursor leads to sodiated and protonated ions, whereas in-source fragmentation can lead to the cleavage of labile leaving groups, such as SEt.

After passing through two ring-electrode ion guides, the ions of interest are mass-to-charge selected by a quadrupole mass filter. Then, the ions enter a quadrupole bender. If no voltage is applied, the ions directly pass through the bender to get to a time-of-flight detector to record mass spectra and to monitor the ion signal. If ±33 V are applied to rods of the quadrupole bender, the ions are bent and enter a hexapole ion trap that is cooled to 90 K by liquid nitrogen in this experiment. The ions of interest are subsequently accumulated in the ion trap and thermalized by collisions with helium buffer gas.

Expansion of pressurized helium into the vacuum by a pulsed Even-Lavie valve leads to the formation of a beam of superfluid helium nanodroplets (0.4 K) that is traversing the ion trap, picking up ions, rapidly cooling them to their equilibrium temperature, and guiding them to the detection region. Here, an infrared (IR) beam generated by the Fritz Haber Institute free-electron laser (FHI FEL) overlaps with the ion beam.

Upon the absorption of resonant photons, vibrational modes of the molecular ions are excited. The ions dissipate the energy to the helium matrix to get back to their ground state. After the absorption of multiple photons, the probed ions are released from the helium nanodroplets and detected by a time-of-flight detector. The ion yield can be plotted as a function of the IR wavenumber, leading to an IR spectrum. Due to the multiphoton absorption process, the intensities in the obtained IR spectrum do not scale linearly. As a first-order correction, the ion signal is divided by the energy of the IR macropulse.

Figures

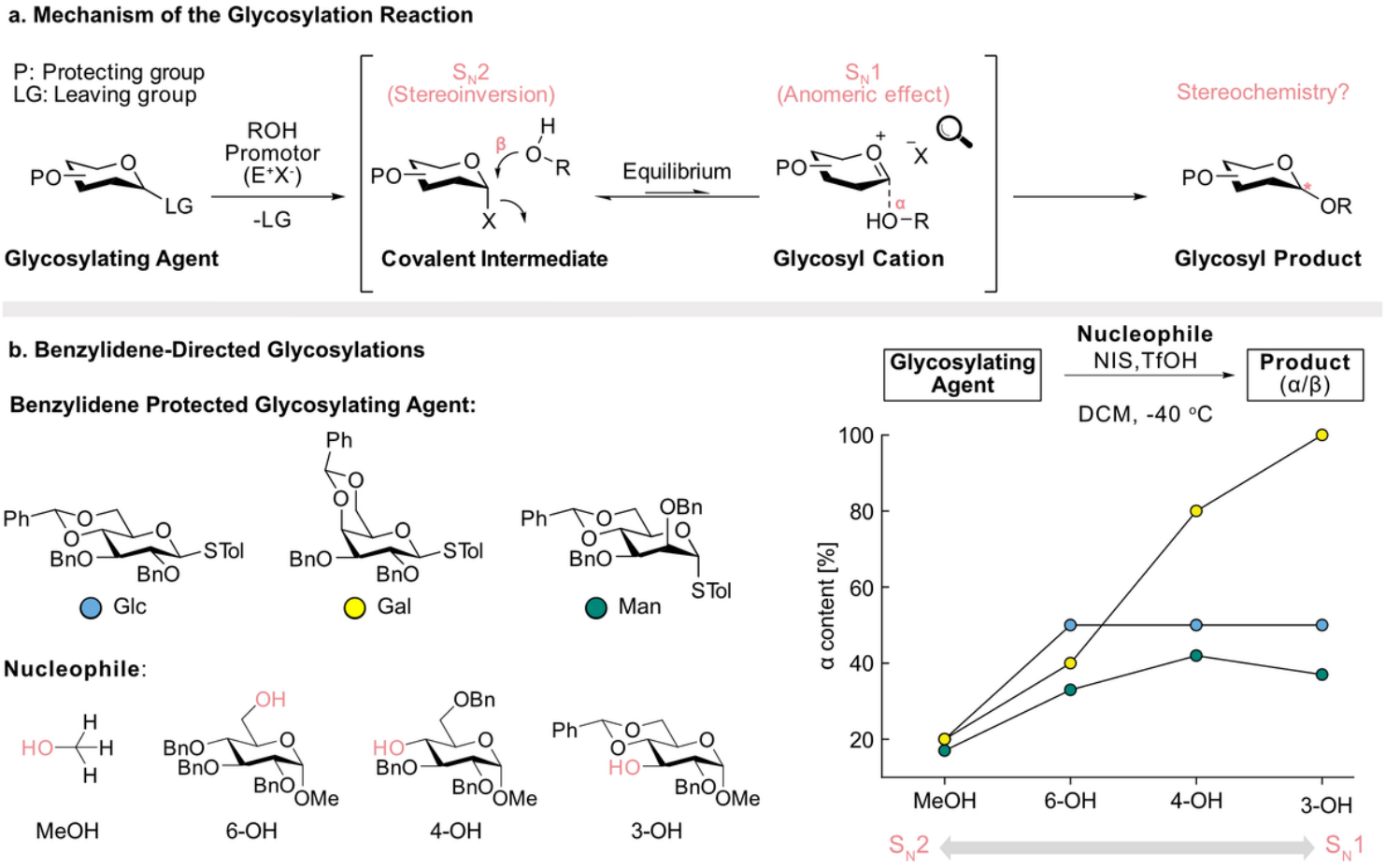

Figure 1

Stereoselectivity in glycosylation reactions. (a) Schematic mechanims of a glycosylation reaction. The stereochemistry of the products is determined by a S_N1-S_N2 continuum. (b) Stereochemical outcome of condensed-phase benzylidene-directed glycosylation reactions reported by Wang.[21,22] Depending on the strength of the nucleophile, the reaction can be directed towards an S_N2- or an S_N1-like mechanism. High β-selectivity is obtained with strong nucleophiles, favoring an S_N2 mechanism, whereas the α-content increases for weak nucleophiles, indicating an S_N1 mechanism.

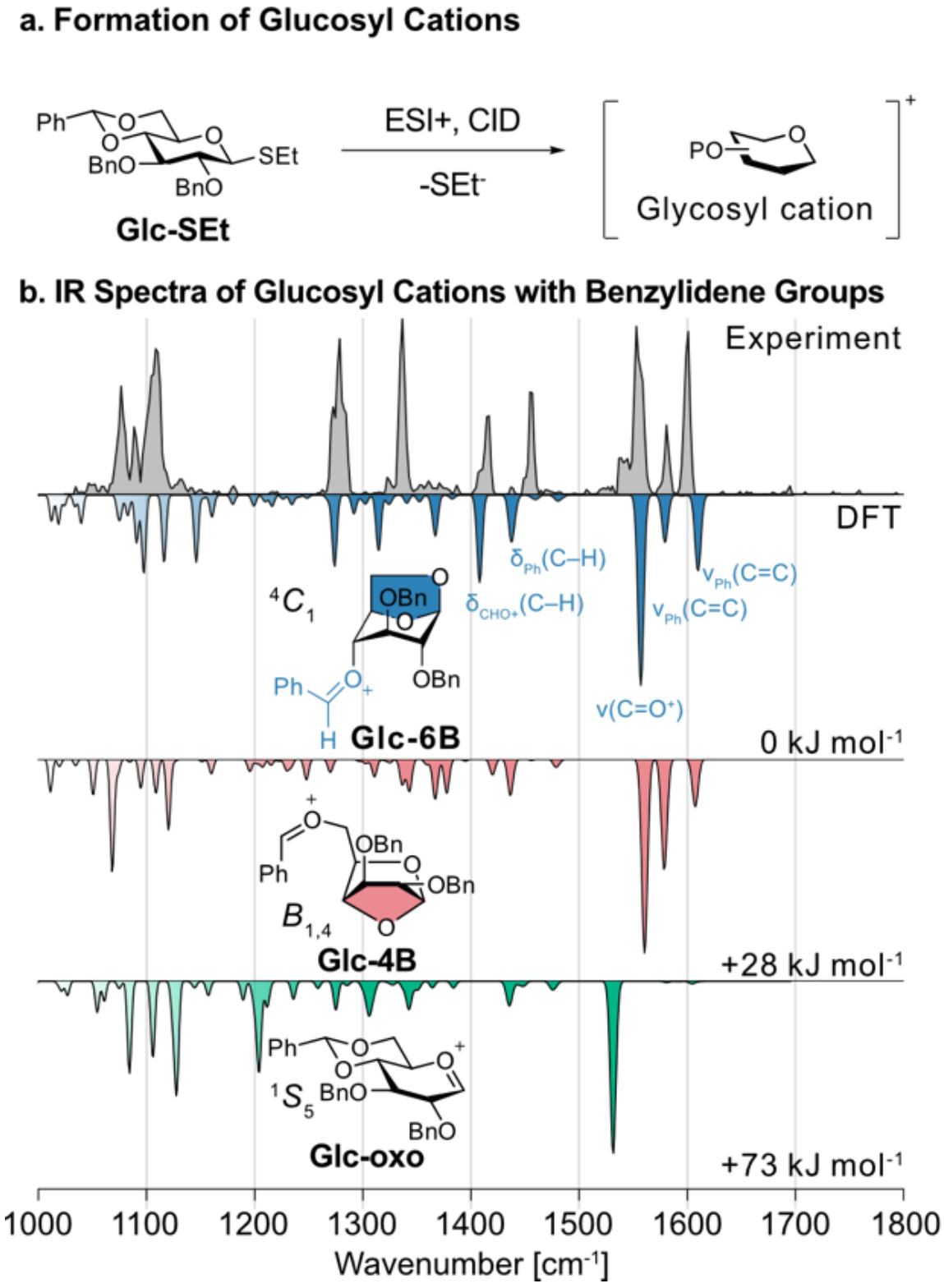

Figure 2

(a) Fragmentation of **Glc-SEt** precursors by in-source fragmentation after electrospray ionization leads to the formation of glucosyl cations. (b) Experimental cryogenic infrared spectrum of a glucosyl cation carrying a benzylidene protecting group (gray). The computed spectra of the lowest-energy 1,6-anhydro cation (blue), 1,4-anhydro cation (red), and oxocarbenium ion (green) are represented in the inverted traces. Ring puckers and relative free energies at 90 K are indicated.

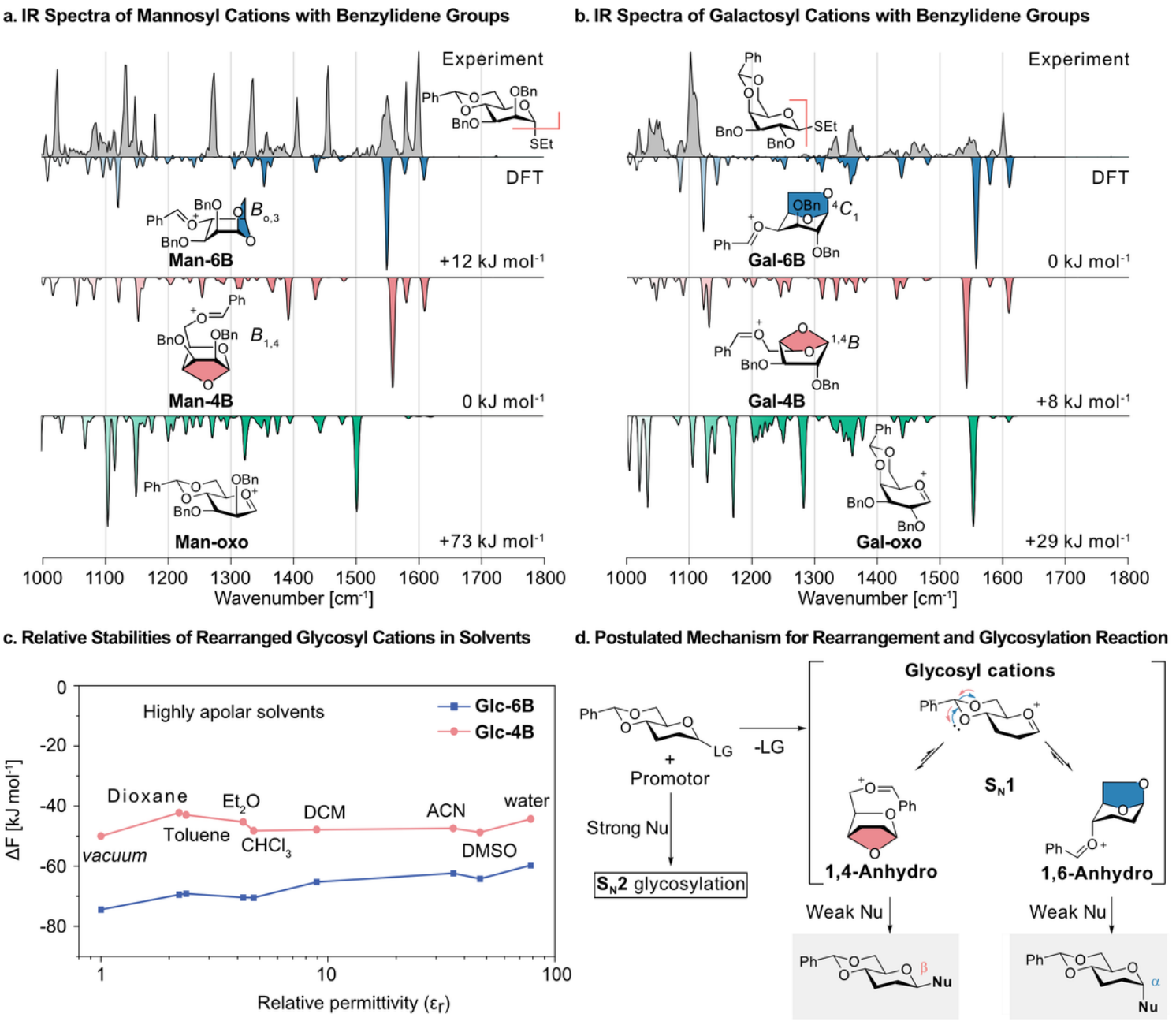

Figure 3

Structures and infrared spectra of glycosyl cations generated from (a) **Man-SEt** and (b) **Gal-SEt** precursors respectively. The experimental cryogenic IR spectrum is shown as a gray trace, whereas computed spectra of the lowest-energy 1,6-anhydro cation (blue), 1,4-anhydro cation (red) and oxocarbenium ion (green) are represented in the inverted traces below. Ring puckers and relative free energies at 90 K are indicated. (c) The relative free energies of **Glc-6B** (shown in blue) and **Glc-4B** (shown in red) calculated using the COSMO solvation model. The calculated free energies are referenced against the lowest-energy oxocarbenium structure **Glc-oxo** (ΔF = 0). The data suggest that the stability of anhydro intermediates is comparable in the gas phase and in various non-polar aprotic solvents. (d) Postulated mechanism for benzylidene-mediated glycosylation on glucose and mannose. The predicted

stereoselectivity for anhydro-type intermediates is correlated with the stereochemical outcome of benzylidene-mediated S_N1-type glycosylation reactions.

Supplementary Files

This is a list of supplementary files associated with this preprint. Click to download.

- SupplementaryInformation.pdf
- NATSYNTH23101161SIxyzCoordinatesgasphase.pdf
- NATSYNTH23101161SIxyzCoordinateswithinsolvents.pdf
- NATSYNTH23101161SI.pdf